Belt Fuser Torque: Modeling Mechanism Drag as Parametric Damping and Corroborating Measurement with EHL Theory

Benjamin Johnson, David Battat; Lexmark International Inc.; Lexington, KY/USA

Abstract

This study pertains to the intrinsic mechanism drag of a belt image fix system which arises mainly due to friction between the heating element and belt. This drag typically increases through module life and can be a main cause of fatigue failure for this type of system. An experimentally obtained parametric damping model is utilized to construct an equation of motion for the system. Properties of the empirical model are used to make inferences regarding the lubrication state in the nip. Mechanism failure due to lubricant starvation is discussed in the context of the model. Finally, reconciliation of the empirical model with elastohydrodynamic lubrication (EHL) theory will be discussed.

Introduction

The torque required to drive a fuser is important for several reasons not unique to image fixing technology. In the short term, accommodating a high torque system requires increased component integrity (and associated cost) to guard against yield failure. Since drive torque typically increases throughout the life of the system, torque can be a main source of fatigue failure as well. Greater drive torque is accompanied by an increased motor power requirement, a topic that resonates with today's emphasis on energy efficiency.

In a belt fuser system, a nip is formed between a backup roll (BUR) whose exterior layer is comprised of an elastomeric material and a heated fusing belt (Figure 1). During normal operation the belt motion is entrained with the motion of the BUR due to friction at that interface. Paper with an electrostatically held image traverses the heated nip thereby melting the toner and fixing the image to the page. A fixed support frame (not shown) inside the belt supports the heater which slides against the inside of the belt supplying heat to the fusing nip. The intrinsic mechanical drag of a ceramic heater in belt image fixing system arises mainly due to sliding friction between the heating element and the belt.

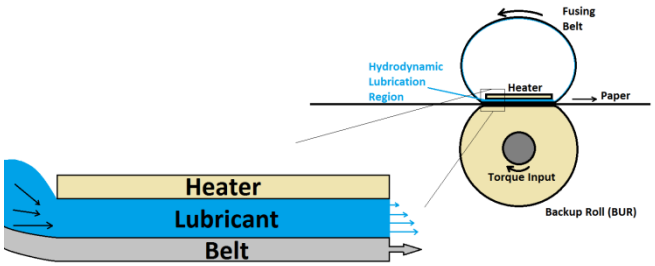

Figure 1. Diagram of a belt fusing system.

While applying lubricant to the heater/belt interface is a common practice, the thermodynamic and tribological implications of doing so are not well understood. Although operating temperature and process speed are observed to influence the drive torque of a given system, an explicit relationship involving the said parameters has not been previously attempted to the authors' knowledge. The general form of such a mathematical relationship is the basis of this work, considering the significance of which allows us to make inferences regarding the lubrication state in the nip.

The goal of this paper is to communicate some of our findings, providing a useful context for making design decisions regarding ceramic heater in belt fuser lubrication. The novelty of our approach is in describing the mechanical drag not in terms of the torque required to oppose it, but instead as the source of the resistance itself: viscous damping. The drag may be modeled as parametric damping which depends upon heater (lubricant film) temperature as well as the rotational speed of the belt. The influence of lubricant temperature and viscosity on fuser driving torque has been examined in the past [1]. In addition, the shear stresses encountered in thin EHL fluid films have been approached both analytically and empirically since the 1950's [2], [3], [4], [5]. The primary difference between the current investigation and previous work is that the corroboration with EHL theory is being attempted in a fusing system as opposed to an off-line test such as ball and plate EHL film thickness measurement.

When system damping is plotted against temperature and belt speed a clear power law relationship is evident. Such a correlation with temperature is not surprising since lubricant viscosity is known to vary in this manner. However, the strong inverse relationship between belt speed and damping reveals our lubrication state as corresponding to the EHL regime and provides a means by which we can estimate the film thickness for a given set of operating conditions. Knowledge of our lubrication state provides a context which allows us to consider mechanism failure modes such as lubricant starvation as well as lubricant oil loss over module life.

Fuser Torque as Viscous Damping

Fuser torque data may be more usefully appreciated by thinking in terms of fuser damping for several reasons. Firstly, torque measurement tends to include some noise, when torque data is divided by measured drive speed cleaner data emerges. This is due to both the torque showing significant dependence on drive speed as well as favorable error propagation which occurs when dividing the somewhat noisy torque signal by the very accurate RPM (driving velocity) signal. Secondly, utilizing a model fitted to the damping data allows for the construction of equations of motion for the system which contain parameterized variables for temperature and drive velocity. Finally, thinking in terms of damping aides the effort to resolve the lubrication state existing in the nip by providing a more direct bridge between actual hardware and EHL theory.

By considering the belt and heater to be parallel plates of a given area separated by a lubricant film under shear (as depicted in

the enlarged portion of Figure 1) a relationship between damping, viscosity, and film thickness may be constructed. The units associated with Equation 3 indicate that a linear relationship should exist between film thickness and damping given that the lubricant behaves as a Newtonian fluid, a conclusion which will be demonstrated in the next section (torque model based on EHL).

$$Viscosity = \frac{Shear\ Traction}{Shear\ Rate}$$

$$= \frac{\left(\frac{Force}{Area}\right)}{\left(\frac{Speed}{Film\ thickness}\right)} = \frac{\left(\frac{N}{mm^2}\right)}{\left(\frac{mm/s}{mm}\right)} = \frac{N}{mm^2} * s = Pa * s \quad (1)$$

$$Damping = \frac{Force}{Speed} = \left(\frac{N}{mm}\right) * s \quad (2)$$

$$Damping = \frac{Viscosity * Area}{Film\ Thickness} = \frac{\left(\frac{N}{mm^2} * s\right) * mm^2}{(mm)} = \left(\frac{N}{mm}\right) * s \quad (3)$$

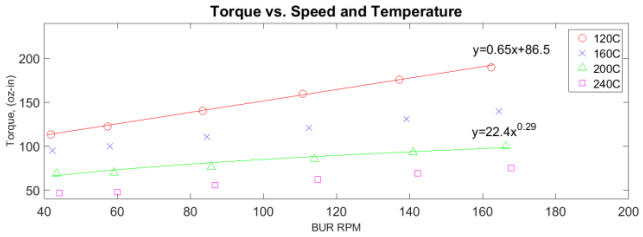

Figure 2. Torque vs. temperature and drive velocity (BUR RPM): Plots of torque vs. drive velocity may lead one to believe that torque varies linearly with BUR RPM. However, a power fit is a more appropriate representation of the underlying hydrodynamic behavior.

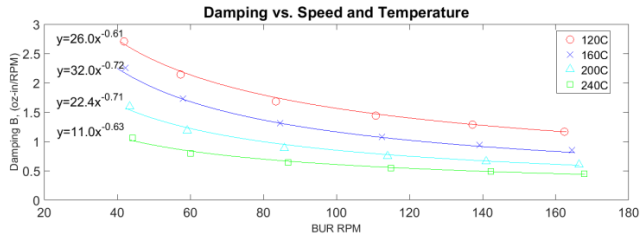

Figure 3. Damping vs. temperature and BUR RPM: Once damping is considered as the source of torque it is clear that damping varies according to a power law with drive (BUR) velocity.

By collectively considering the curves from Figure 3, a two dimensional model of damping vs. speed and temperature may be constructed of the form

$$B = aT^b\omega^c \quad (4)$$

Where B is damping, T is temperature, and ω is driving velocity, while a, b, and c are fit coefficients. A plot of such a fitted surface may be found in Figure 4.

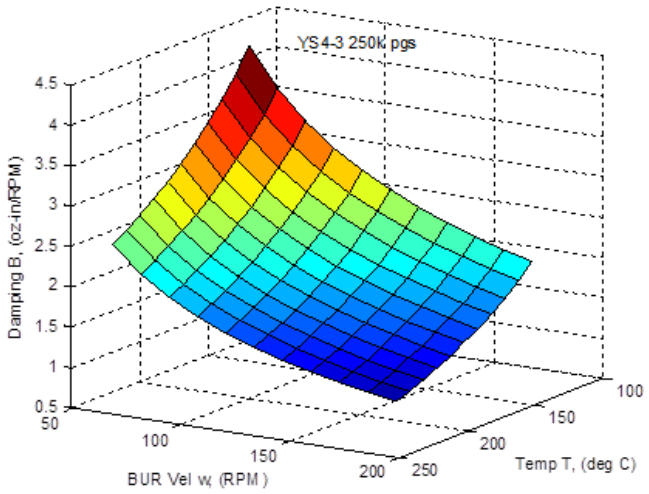

Figure 4. Damping vs. temp and BUR rpm: Model of the form $B = aT^b\omega^c$ fit to measured damping data.

The temperature and speed dependence of damping explains the desire to reduce drive velocity until reaching a particular temperature [1] and provides a means to predict system friction for any given temperature/speed combination.

Torque Model Based on Elastohydrodynamic Lubrication (EHL)

The classical expression for grease thickness may be calculated from the lubrication theory [3].

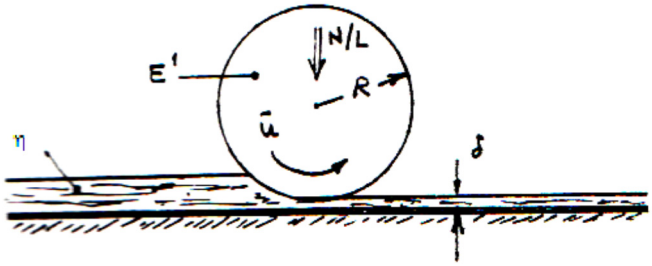

Figure 5. Diagram of elastohydrodynamic grease film as described by Equation 5.

In dimensional form

$$\delta = 1.6\alpha^{0.6}R^{0.43}(E')^{0.03}(\eta\bar{u})^{0.7}(N/L)^{-0.13} \quad (5)$$

where

δ = Grease film thickness in the nip

N = Total load

L = Roll length

η = Grease viscosity at operating temperature and shear rate

$\bar{u}$ = Mean surface speed $(u_1+u_2)/2$

R = Equivalent radius $1/R = 1/R_1+1/R_2$

E' = Equivalent modulus of elasticity

$1/E' = (1/2)\,(\{1-\upsilon_1^2\}/E_1 + \{1-\upsilon_2^2\}/E_2)$

α = Pressure-viscosity exponent takes into account the increase in viscosity with pressure $\eta=\eta_o\exp(\alpha p)$ where p is pressure and η_0 the viscosity prior entry into contact.

Equation 5 indicates that grease thickness, δ, in the nip is affected mostly by grease viscosity and belt speed, moderately by BUR radius, and very weakly by load and equivalent modulus. An expression may be developed for the viscous torque: the motion of the grease is brought about by the moving belt. The pressure gradient dp/dx = 0, so that the fluid has a straight line velocity distribution. Thus, the shear stress on the belt is given by

$$\tau = \eta \frac{du}{dy} = \eta \frac{U}{\delta} \tag{6}$$

The torque increases as grease film thickness decreases, as shown in Equation 7.

$$\tau = \frac{\eta U}{\delta} Nip \cdot L \cdot R_{BUR} \tag{7}$$

For moderate loading the nip may be approximated by the regression

$$Nip = 1.574h\left[\frac{4}{\pi}\frac{N}{L}\frac{R_{BUR}(1-\nu)^2}{Eh^2}\right]^{0.32} \tag{8}$$

In the above, h is BUR rubber thickness, $R = R_{BUR}$, $1/E' = (1-\nu_2)/2E$, and $U=2\bar{u}$, i.e. belt speed is twice the average speed. Using Equations 5, 7, and 8, the torque can be expressed as

$$T = 2.644\alpha^{-0.6}(\eta\bar{u})^{0.3}N^{0.45}L^{0.55}h^{0.37}R^{0.89}(E')^{-0.35} \tag{9}$$

Equation 9 indicates that torque is most affected by BUR radius and roll length, followed next by load and, to a lesser extent by rubber thickness and modulus. Grease viscosity and belt speed are least important for torque, being raised only to the power 0.3 versus the film thickness (Equation 5), where the same product was raised to the power 0.7.

A comparison of Equation 9 with Figure 2 shows good agreement: the experimental torque depends on speed to the power 0.3, in good agreement with the model's prediction (Equation 9), where dependence is also to power 0.3.

Viscosity can depend on speed via shear rate. Since the predicted value is around 0.3, this suggests that for the lubricants tested, the viscosity does not depend on the shear rate. Therefore, in the range tested, the lubricants are operating in the Newtonian regime, in which case, the viscosity can be expressed in terms of an Arrhenius relationship. Plotting ln of the torque versus 1/T°K yields a straight line with a slope proportional to the activation energy: Ea = 9460.77 cal/mole, which is a measure of the rate of change with temperature.

Using Equation 9 for torque, a damping coefficient, B, can be defined explicitly as given in Equation 10. Thus, B is determined as a function of the speed and the parameters involved in the lubrication system. Again theory and measurements agree well. Figure 3 shows that the dependence of damping B on speed is between -0.6 and -0.8, whereas the theoretical value according to Equation 8 is -0.7.

$$B = 2.644\alpha^{-0.6}(\eta)^{0.3}\bar{u}^{-0.7}N^{0.45}L^{0.55}h^{0.37}R^{0.89}(E')^{-0.35} \tag{10}$$

Comparison with Equation 4 shows that index $c = -0.7$ and index α is a constant coefficinet which captures the unvaried terms in Equation 10.

On this basis, the motion of the belt assembly can be described by Equation 11. For a given external torque, τ, the equation describes the evolution of motion from rest to an ultimate steady-state angular velocity, i.e. the equation represents the transient evolution of the motion.

$$J\ddot{\theta} + B\dot{\theta} + K\theta = \tau \tag{11}$$

Equations of Motion

For the sake of simplicity the problem may be reduced from a rotational system to a translational system with 1 degree of freedon (DOF) and nonlinear damping. The 1 DOF assumption is justified as long as the fuser is undergoing normal operation where no relative sliding motion exists between the belt and BUR. The belt is considered to be a rigid mass connected to the input (driving velocity) through a linear spring which represents the torsional stiffness of the gear train and BUR core/rubber combination.

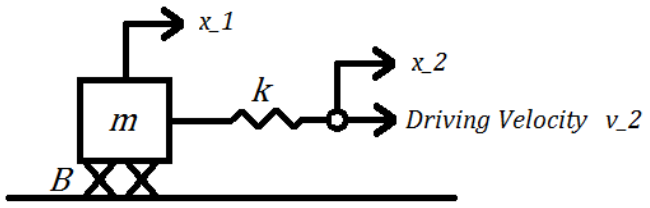

Figure 6. System diagram.

For this system, equations of state may be written as follows:

$$\dot{x}_1 = v_1 \tag{12}$$

$$\dot{v}_1 = \frac{1}{m}[k(x_2 - x_1) - Bv_1] \tag{13}$$

$$\dot{x}_2 = v_2 \tag{14}$$

$$\dot{v}_2 = 0 \tag{15}$$

Where x_1 is belt position, v_1 is belt velocity, x_2 is driving position, v_2 is driving velocity, m is belt mass, k is the stiffness of the connection between the driving velocity and the belt, and B is damping coefficient. It should be noted that $\dot{v}_2 \neq 0$ when drive velocity is varied to model system response to that type of input. Replacing angular velocity ω in Equation 4 with its translational equivalent v_1 (from Equation 12) and applying to Equation 13 provides:

$$\dot{v}_1 = \frac{1}{m}[k(x_2 - x_1) - v_1(aT^b v_1{}^c) \tag{16}$$

This set of equations (12, 14, 15, and 16) may be solved for a given time varying temperature profile and set of initial conditions

once fit coefficients are established in Equation 16 for a given fuser and values for k and m have been estimated.

Stick-Slip Motion at Low Speed

At a combination of low speeds and high temperatures torque may be measured to increase with decreasing velocity. In terms of damping this is equivalent to the power dependence of damping on belt speed transitioning through -1 from above (Figure 7). Since

$$\tau = Bv_1 \tag{17}$$

and

$$B = B_0 {v_1}^n \tag{18}$$

Where B_0 and n are equivalent to fit coefficients a and c in Equation 16 respectively and may be obtained from trend lines on Figure 7. Appling Equation 18 to Equation 17

$$\tau = B_0 {v_1}^{1+n} \tag{19}$$

From Equation 19 it is clear that when $-1 < n < 0$ torque will increase with increasing belt speed but when $n < -1$ torque will decrease with increasing belt speed. This change in behaviour indicates the transition from hydrodynamic lubrication to boundary or mixed lubrication which may be interpreted with the help of a plot of friction coefficient vs. Sommerfield number (Figure 8).

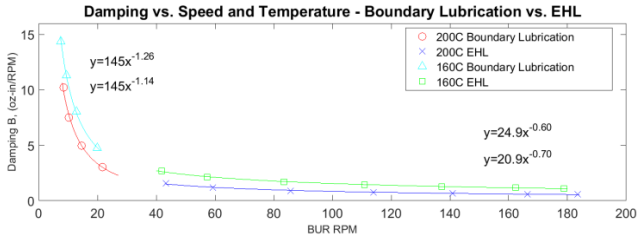

Figure 7. Damping vs. temperature and BUR RPM: Exponent on BUR RPM is less than -1 in boundary lubrication region and between 0 and -1 in the EHL region.

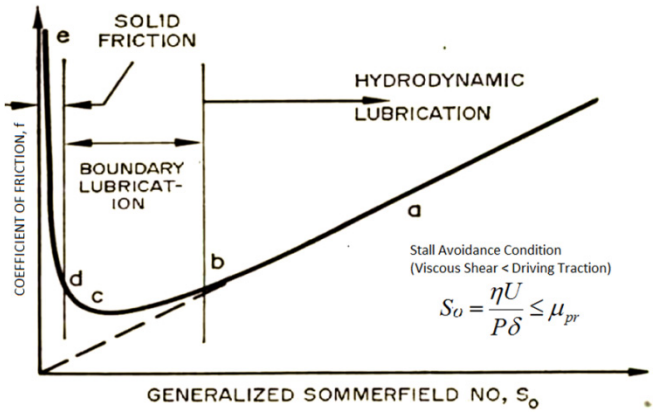

Figure 8. Friction coefficient vs. Sommerfield number: The local dependence of frictional drag on the Sommerfield number can be used to distinguish the boundary and hydrodynamic lubrication regions. [6]

Assuming no slippage occurs between the BUR and belt, the friction between the belt and heater can exceed the input torque for sufficiently low speed causing the belt to stall. This is exemplified by the Sommerfield number, S_o , which may be obtained from the equation shown in Figure 8. The diagram in Figure 8 defines the various lubrication regimes, and shows the boundary delineating driving from sticking or stall. For a given S_o value, Figure 8 defines the limit of the coefficient of friction (CoF) between the belt and heater. If the friction force is higher than the input torque, the belt will stall, and if lower, then the belt will rotate.

In the hydrodynamic region, damping values are measured to vary with velocity to the power of approximately that which is suggested by EHL theory [3], or -0.7. Referencing the state equations presented earlier this corresponds to $c = -0.7$ in Equation 16. For constant temperature and estimated values of 1, 1000, and 50 for m, k, and B_0 respectively this reduces Equation 16 to

$$\dot{v}_1 = 1000(x_2 - x_1) - 50v_1{v_1}^{-0.7} \tag{20}$$

$$= 1000(x_2 - x_1) - 50{v_1}^{0.3} \qquad v_1 > 1 \tag{21}$$

The hydrodynamic region must be bounded by a minimum belt velocity which measured data has suggested occurs at approximately $v_1 < 1$ for system units (in, oz, sec). It should be noted that the above parameter values are approximate and are intended to provide a tangible basis by which to simulate the stick-slip phenomenon. The estimated values are to be varied with the intent of displaying their relative influence on the system behaviour. The value of c on the other hand is obtained experimentally for both the hydrodynamic and mixed lubrication regions and will not be varied.

In the boundary or mixed lubrication region (i.e. when $v_1 < 1$) c is measured to assume a value of approximately -1.2 which impacts $\dot{v}_1$as follows:

$$\dot{v}_1 = 1000(x_2 - x_1) - 50v_1{v_1}^{-1.2} \tag{22}$$

$$= 1000(x_2 - x_1) - 50{v_1}^{-0.2} \qquad v_1 < 1 \tag{23}$$

The negative exponent on $v_1$in Equation 23 means that term will approach infinity as belt velocity goes to zero. Of course in reality this is not the case and the damping force will approach some maximum value at $v_1 = 0$. In order to build a model which accommodates reality as well as numerical simulation of stick-slip motion a third region must be included in the analysis. Work done by Do, Ferri, and Bauchau gives an in depth and well-articulated treatment of the difficulties associated with modelling various friction models undergoing stick-slip motion [7]. Their solution is to include a term of the form $Ae^{-(v_1/v_s)}$ where $v_1 < v_s$ which they attribute to Canudas de Wit et. al [8]. The term v_s is some very small velocity below which the mass is assumed stuck or to be undergoing microslip. Applying the said term to Equation 23 provides

$$\dot{v}_1 = 1000(x_2 - x_1) - Ae^{-(v_1/v_s)} \qquad v_1 < v_s \tag{24}$$

where the condition

$$|1000(x_2 - x_1)| > |Ae^{-(v_1/v_s)}| \qquad v_1 < v_s \tag{25}$$

must also be satisfied in order to induce a slip (i.e. the spring force must exceed the damping force). On the other hand, when the spring force is not sufficient to overcome the sticking friction, that is

$$|1000(x_2 - x_1)| < |Ae^{-(v_1/v_s)}| \qquad v_1 < v_s \tag{26}$$

then

$$\dot{v}_1 = 0 \tag{27}$$

Which means when the spring force is small and the belt velocity v_1 crosses the stick threshold v_s from above, v_1 will retain a small unchanged value until it is again overcome by the spring force. This motion constitutes the previously mentioned microslip.

The term A first appearing in Equation 24 may be utilized to smooth the handoff between Equations 23 and 24, that is, when transitioning through the critical speed v_s. The term A can be seen to depend upon values chosen for both B_0 and v_s and may be determined by solving:

$$Ae^{-(v_s/v_s)} = B_0 {v_s}^{-0.2} \tag{28}$$

or

$$Ae^{-1} = 50(0.01)^{-0.2} \qquad A \cong 341.4 \tag{29}$$

for the baseline case of $B = 50$ and $v_s = 0.01$. In order to make the sign of the newly introduced term correct the following modification must also be applied:

$$\dot{v}_1 = 1000(x_2 - x_1) - sgn(v_1) * (341.4)e^{-|\frac{v_1}{v_s}|} \tag{30}$$

Simulations

Equations 12, 14, 15, 21, 23, 24, 27, and 30 as well as conditions described by Equations 25 and 26 were simulated with the Runge-Kutta based method ode45 in Matlab for a range of values for the system parameters k, B_0, and driving velocity v_2. A plot of what will be considered the baseline case is found in Figure 9.

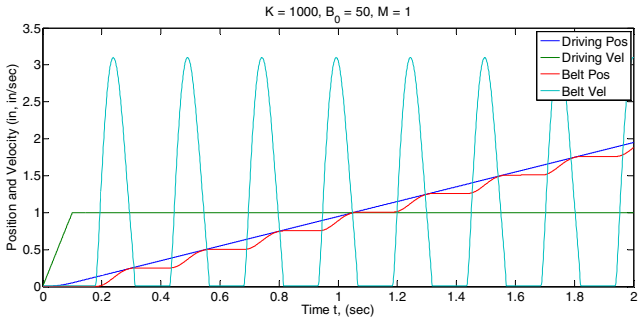

Figure 9. Baseline case: $k = 1000$, $B_0 = 50$, $m = 1$, driving velocity $v_2 = 1$.

Increasing the stiffness ***k*** may be seen to affect the stick-slip frequency in an approximately proportional linear fashion. Increasing spring stiffness also reduces the slip velocity amplitude.

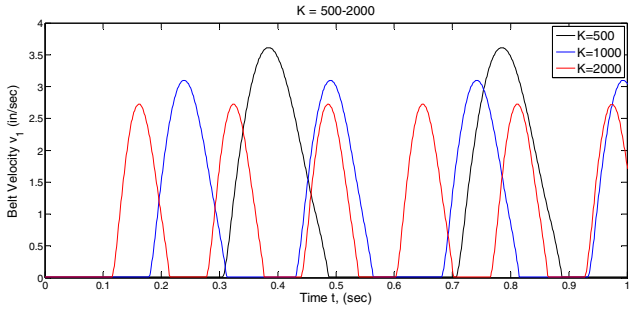

Figure 10. Effect of varying spring stiffness: $k = 500 - 2000$, $B_0 = 50$, $m = 1$, driving velocity $v_2 = 1$.

Varying the constant portion of the damping coefficient B_0 affects both the slip velocity and frequency due to it's impact on A (used in Equations 24, 25, 26, and 30) which dictates the sticking friction.

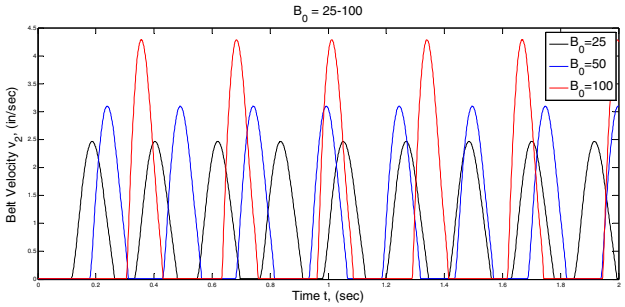

Figure 11. Effect of varying B_0: $k = 1000$, $B_0 = 25 - 100$, $m = 1$, driving velocity $v_2 = 1$.

Increasing driving velocity v_2 may be seen to have a similar effect to increasing spring stiffness however increasing drive velocity leads to an increase in slip velocity amplitude.

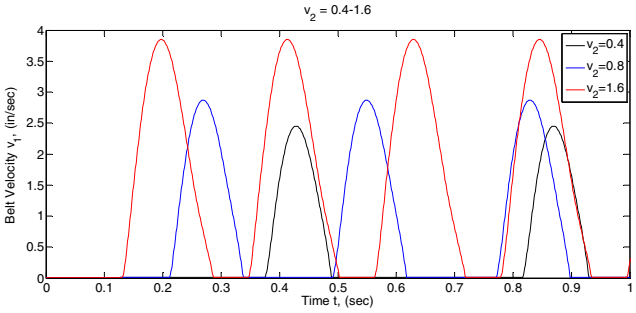

Figure 12. Effect of varying drive velocity: $k = 1000$, $B_0 = 50$, $m = 1$, driving velocity $v_2 = 0.4 - 1.6$. Increasing drive velocity leads to an increase in both slip frequency and slip velocity amplitude.

System Hysteresis

The parametric damping system model described herein may be shown to exhibit hysteresis, the effect of which may potentially be utilized to avoid the stick-slip phenomenon in certain situations. When required to operate at a velocity near the mixed/EHL transition due to external factors, simulation results indicate that it should be beneficial to intentionally overshoot the desired velocity and subsequently approach it from above. This effect is illustrated in Figures 13 and 14 where the mixed/EHL transition velocity is 1 in/sec in both cases.

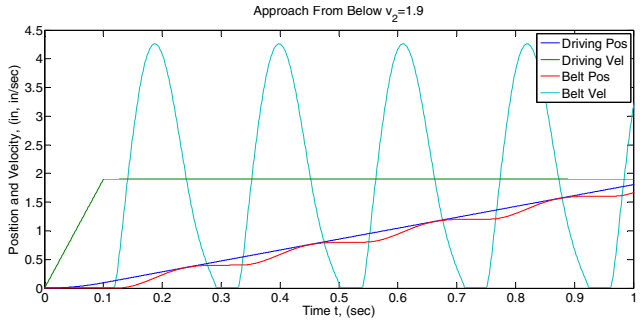

Figure 13. Hysteresis, approaching from below: Even for a driving velocity which is 1.9x the mixed/EHL transition speed stick-slip motion is maintained in the steady state when approaching from below. Baseline case considered.

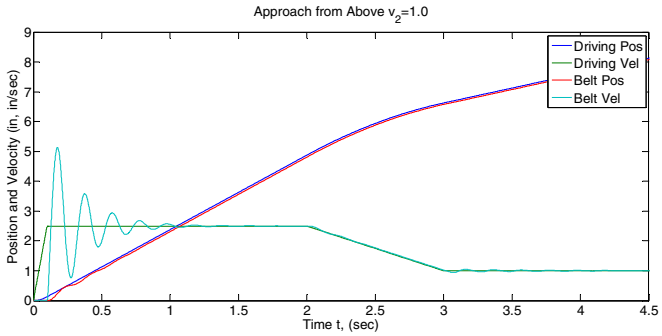

Figure 14. Hysteresis, approaching from above: A velocity of 1.0 in/sec is achieved without exhibiting stick-slip motion in the steady state when velocity is first intentionally made to overshoot to 2.5x the mixed/EHL transition velocity. Again, baseline case considered.

References

[1] K. Okuda, Y. Tomoyuki, A. Hayakawa, M. Takano, D. Fukuzawa, and A. Abe, Image Heating Apparatus, Canon Kabushiki Kaisha, assignee, US Patent 5852763, 1998.

[2] D. Dowson and G. R. Higginson, "A Numerical Solution to the Elastohydrodynamic Problem," Jour. Mech. Eng. Sci, vol. 1, p. 6, 1959.

[3] D. Dowson and G. R. Higginson, Elastohydrodynamic Lubrication, the Fundamentals of Roller and Gear Lubrication, Oxford, Great Britain: Pergamon Press, p. 190, 1966.

[4] S. Hurley and P.M. Cann, "Grease Composition and Film Thickness in Rolling Contacts," NLGI Spokesman, vol. 63 (4), pp. 12-22, 1999.

[5] J. de Vicente, "Behaviour of Complex Fluids between Highly Deformable Surfaces: Isoviscous Elastohydrodynamic Lubrication," Accessed online from: Marie Curie Fellowship Association Annals at http://www.mariecurie.org/annals, vol. 4, 2005.

[6] D. F. Moore, The Friction and Lubrication of Elastomers, Oxford, Great Britain: Pergamon Press, p. 95, 1972.

[7] N. Do, A. Ferri, and O. Bauchau, "Efficient Simulation of a Dynamic System with LuGre Friction," Jour. of Comp. and Nonl. Dyn, vol. 2, pp. 281-289, 2007.

[8] C. Canudas de Wit, H. Olsson, K. J. Astrom, and P. Lischinsky, "A New Model of Control of Systems with Friction," IEEE Trans. Autom Control, vol. 40 (3), pp. 419-425, 1995.

Author Biography

Ben Johnson completed a BSME at the University of Kentucky in 2008, joining Lexmark later that year. After a short assignment in ink-jet printhead development he has worked in fuser development since 2010. Ben is an inventor on 1 published patent and 7 others either pending or soon to be filed. He is currently pursuing an MSME with a focus in finite element analysis at his alma mater part-time and plans to graduate in the fall next year.